Brazilian Journal of Physics (2021) 51:329–338
https://doi.org/10.1007/s13538-020-00837-9

SOCIEDADE BRASILEIRA DE FÍSICA

ATOMIC PHYSICS

Characterization of the Collimation of an Atomic Beam with a Monochromatic Quasi-resonant Laser

P. G. S. Dias[1] · M. A. F. Biscassi[1] · P. H. N. Magnani[1] · R. F. Shiozaki[1] · Ph. W. Courteille[2] · R. Celistrino Teixeira[1]

Received: 27 February 2020 / Accepted: 26 November 2020 / Published online: 4 January 2021

Abstract
In this article, we measure the collimation of an atomic beam of strontium that emerges from an array of microtubes installed at the output of an atomic oven, through the characterization of the beam fluorescence caused by a monochromatic laser beam close to resonance with a strontium electronic transition, as a function of the transverse position at the atomic beam and the light detuning. We develop a theoretical model to obtain the total fluorescence rate as a function of the collimation of the atomic beam, the temperature of the atomic oven, and the laser frequency. Collision effects between the atoms, and the atoms with the recipient walls, are included to make the model realistic. The method and theory developed are useful to laboratories willing to implement such atomic sources, for experiments with atomic beams or cold atomic samples.

Keywords Atomic beam · Strontium · Atomic physics · Atomic fluorescence

1 Introduction

The field of atomic physics has undergone a major revolution with the advent of various laser cooling techniques for atoms. Doppler cooling or optical molasses [1, 2], the Zeeman decelerator [3], the magneto-optical trap [4], Sisyphus cooling [5, 6], and sideband cooling [7] are examples of techniques that are used in current experiments to obtain cold and ultra-cold atomic samples, of temperatures typically of the order of microKelvin or lower, beginning from atomic gases at room temperature or higher. Commonly, to obtain such low temperatures, more than one of the above techniques must be combined. These cold and ultra-cold atomic gases have made great progress in fundamental physics, of which a short list of examples comprises the obtaining of neutral atomic Bose-Einstein condensates [8, 9] and degenerate quantum fermionic gases [10], the simulation of Hamiltonians and solid state models [11], the study of quantum dipolar gases [12], Anderson's location of matter waves [13], and the observation of various light-matter interaction phenomena as subrradiance [14].

Several atomic sources can be used to charge the first cooling stage of a cold atoms experiment: atomic dispensers [15], atomic gases at room temperature, collimated atomic beams. The choice of the atomic source for the experiment respects criteria such as available total power of laser light, dimensions of the vacuum system, and available electronic transitions of the atomic species. Collimated atomic beams from hot sources are a good choice for atomic species with low vapor pressure at room temperature, and should be combined with a Zeeman decelerator to reduce their average speed. Before being used for loading cold and ultra-cold atomic samples, collimated atomic beams were used as such for several studies on the interaction between atoms and light: Atomic spectroscopy of fine and hyperfine levels [16], Ramsey interferometry [17], implementation of atomic clocks [18], and hydrogen masers [19, 20], a precursor of the laser that verified the possibility of coherent radiation amplification by resonant systems. When highly collimated, the transverse Doppler effect of the atoms can be reduced such as to allow for accessing the natural linewidth of an atomic transition. This possibility was used in the first experiments of optical pumping between electronic levels [21] and for the measurement of the fluorescence spectrum of atoms subject to high light intensities [22].

P.G.S. Dias and M.A.F. Biscassi contributed equally to this work

✉ R. Celistrino Teixeira
teixeira@df.ufscar.br

[1] Departamento de Física, Universidade Federal de São Carlos, Rodovia Washington Luís, km 235 - SP-310, São Carlos, SP, 13565-905, Brazil

[2] Instituto de Física de São Carlos, Universidade de São Paulo, São Carlos, SP, 13560-970, Brazil

Due to the importance of atomic beams, the optimization of their collimation and flow has been intensively studied in the past. The simplest way to obtain a collimated atomic beam is to start with an effusive flow of atoms, which emerge from an aperture in the surface of a container containing a gas of the atomic species in question (usually heated to increase the saturating vapor pressure of the source solid, and therefore called an atomic oven), and to collimate it by placing a diaphragm of diameter d at a distance l from the aperture, causing a reduction in the transverse beam velocity distribution of the order of d/l. However, only a fraction of atoms of the order of $(d/l)^2$ is present in the solid angle that passes through the diaphragm, which means that most atoms will be lost by this method. In order to increase the proportion of atoms present in the useful solid angle of the effusive flow, an array of microtubes can be installed at the oven output [19]. These microtubes have a typical diameter of a few tens or hundreds of micrometers, and thus have a length much larger than their diameter (which we will also call respectively l and d). For low gas pressures in the oven, these microtubes act by selecting the direction of the velocities of the atoms that manage to escape from it, since the vast majority return after some collisions with the walls of the microtubes. In this way, the collimation of the beam is still of the order of d/l, but now the atoms that escape are mostly present in the collimated beam; furthermore, the atomic flux in the center of the beam is not reduced when compared to the value in the center of the effusive beam. For high oven pressures, however, collisions within the microtubes tend to decrease the flow in the center of the beam, and increase their divergence [23], reducing the advantages of this assembly. The calculation of the velocity distribution profile of atoms by an array of microtubes in the high-pressure regime should include collisions between their constituents, and between their constituents and the walls of the microtubes, and in general only agrees qualitatively with the real behavior of a system [23]. Therefore, experimental characterization of the atomic beam obtained by microtubes is necessary.

In this article, we describe the experimental characterization of a neutral strontium beam, produced from microtubes installed at the output of an oven, which we used in our experiment as an atomic source of an experimental machine capable of preparing cold samples of bosonic strontium. For the characterization of the spatial distribution of velocities of the beam, we measure the fluorescence of the atoms subject to a laser beam crossing the atoms at different angles, as a function of the atomic position and the frequency of the light. For the quantitative analysis of the data obtained, we developed a model that takes into account the interaction between the atoms and the light, the output profile of the oven, and possible collision effects among atoms and within the container walls. The characterization method developed here can be directly employed in the characterization of experimental systems for different atomic species.

This paper is organized as follows: In Section 2, we present the experiment which allowed us to obtain the main characteristics of the atomic beam from fluorescence measurements made with a narrowband laser. In Section 3, we develop a theoretical model that we will compare to our results in order to deduce the relevant parameters of our beam, such as divergence and average speed. In Section 4, we analyze and discuss the experimental data, and in Section 5, we present the main conclusions of this work.

2 Experiment

The main experiment where the atomic oven described here is inserted is capable of cooling strontium atoms to a temperature of 10 μK and is described in detail in [24]. Here, we will focus on the first section of the experiment, which produces a beam of hot atoms that will feed the next stages, shown in Fig. 1. The source of atoms is an oven containing metallic strontium, which is heated to a temperature of $T = 835$ K by resistors installed outside the oven. In order to minimize the power required to maintain such temperatures, we wrap the oven and the external resistances with an insulating ceramic, wrapped in turn with glass wool and aluminum foil, in order to minimize heat losses to the environment. The temperature measurement of the oven is made with a thermocouple installed outside the oven, inside the layers of thermal insulation. The oven is connected to a first high vacuum chamber, maintained by ion pumping at a pressure of 2.10^{-8} mbar, through an array of microtubes with internal diameter 130 μm and length 8 mm, arranged in a 4-mm diameter circle. These microtubes are produced by cutting surgical needles with a CO_2 laser. Figure 2 shows a picture taken under a microscope of the microtube array. It is in this first high vacuum chamber that the atomic beam characterization measures were performed.

The high vacuum chamber immediately after the oven is equipped with viewports, which allow to send a laser beam of linear polarization, represented in Fig. 3a, that propagates in the positive direction of the z axis and whose center crosses the point $\vec{r} = (L, 0, 0)$ (see Figs. 1 and 3a for the origin of the coordinate system, at the center of the oven output). This beam is obtained from a commercial laser from Toptica, model SHG-Pro, that produces narrowband laser light with wavelength around $\lambda_0 = 461$ nm. The typical spectral width of light is < 1 MHz. The frequency of this laser beam is scanned around the electronic dipole transition of ^{88} Sr between the fundamental level $(5s^2)^1S_0$

and the excited level $(5s5p)^1P_0$, of wavelength $\lambda_0 = 460.82$ nm and natural width $\Gamma/(2\pi) = 30.5$ MHz. It is important to note that the solid strontium sample contained in the oven has an isotope distribution equal to that found in nature; therefore, 82.6% of the beam is made of ^{88}Sr. The other most frequent isotopes, ^{86}Sr with 9.8% and ^{87} Sr with 7.0%, have electronic resonances between the levels $^1S_0$ and $^1P_0$ displaced from the ^{88}Sr one by 125 MHz and 60 MHz, respectively.

The laser beam is Gaussian and collimated in the region where it crosses the atomic beam, with a Gaussian waist (the beam radius at $1/e^2$) $w = 7.9$ mm, and total power $P = 250$ µW. Since the atoms are subject to a quasi-resonant light beam, they will absorb and re-emit photons at this wavelength, causing a fluorescence that is visible in our experiment to the naked eye. To measure it quantitatively, we installed a CCD camera, positioned at $(L, -L_c, 0)$, with $L_c = 22$ cm, and directed to the atoms, whose signal in each pixel is proportional to the amount of incident light. A 25-mm focal length lens combines the image of the $y = 0$ plane, centered on $(x, z) = (L, 0)$, on the CCD. The distance L_c from the camera to the atoms is much greater than the dimensions of the excitation region by the laser. The camera is, therefore, at a similar distance from each atom, and we can consider that the total solid angle of the fluorescence of each one captured by the camera is the same. This is important, as it means that the camera signal is directly proportional to the fluorescence created by each atom in the beam.

In order to interpret the data obtained, extracting in particular the divergence of the atomic beam, we developed the model that we describe in the next section.

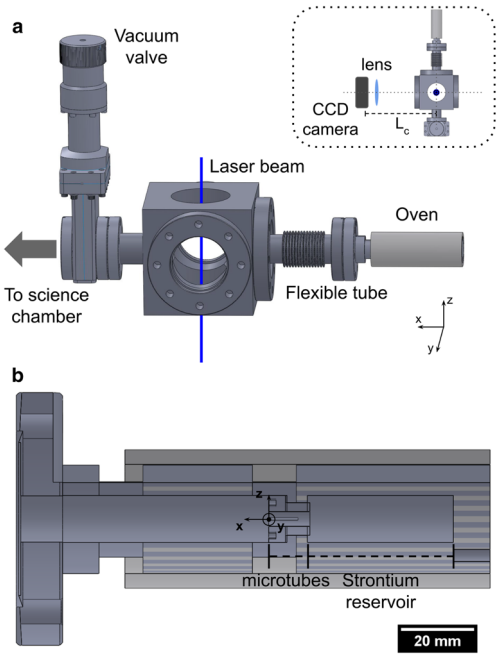

Fig. 1 Design of the experimental assembly of the strontium oven. **a** Overall view of the vacuum apparatus, where we also indicate the coordinate system used in all calculations. At the right, we find the oven, where we create a strontium vapor by heating metallic strontium. The atoms that emerge from the oven pass through a flexible tube before reaching the vacuum chamber, equipped with viewports, through which we send the laser beam used to characterize the collimation of the atomic beam. The vacuum valve separates the oven section from the science chamber, not shown in the figure, where we produce the ultra-cold atomic cloud. A lens conjugates the image of the $y = 0$ plane, which contains the laser beam that makes the atoms fluoresce, in the plane of the CCD camera. **b** Cross-section of the oven, showing the metallic strontium reservoir and the micro-tubes that separate it from the high vacuum region. The coordinate system indicates the direction of each axis, and is here positioned at the origin that we use for the theoretical model

3 Model

3.1 Number of Photons Scattered per Atom

An atom interacting with light of frequency close to one of its electronic dipole transitions has a photon scattering rate that is given by [25]:

$$\gamma = \frac{\Gamma}{2} \frac{s_0}{1 + s_0 + \frac{4\Delta^2}{\Gamma^2}}. \quad (1)$$

In this equation, Γ represents the natural width of the dipole transition, $\Delta = \omega - \omega_0$ is the detuning of the light frequency seen by the atom, ω, with respect to the frequency ω_0 of the atomic transition, and s_0 is the light saturation

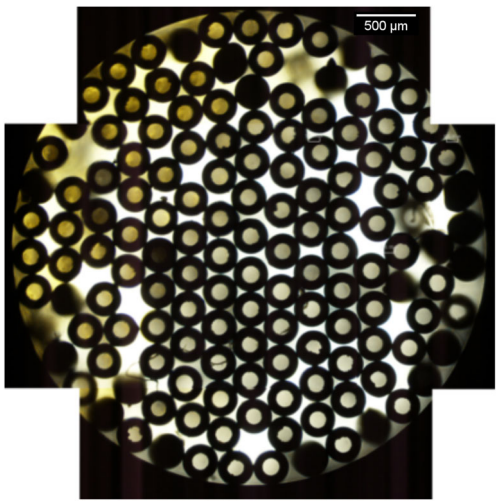

Fig. 2 Picture taken by microscope of the microtube array installed at the output of the strontium oven. The spatial scale of the image is indicated. The external diameter of each microtube is equal to 300 µm, and the internal diameter is equal to 130 µm. The diameter of the tube in which the microtubes are inserted is equal to 4 mm

parameter at resonance. The saturation parameter is a linear function of the intensity of the incident light according to:

$$s_0 = \frac{I}{I_{\text{sat}}}\,. \tag{2}$$

The constant $I_{\text{sat}} = \hbar\Gamma\omega_0^3/(12\pi c^2)$ [25] is called the saturation intensity of the transition.

In our experimental system, shown schematically in Fig. 3a, the laser beam has an intensity profile given by:

$$I(x, y) = I_c\, \mathrm{e}^{-2[(x-L)^2+y^2]/w^2}\,, \tag{3}$$

where:

$$I_c = \frac{2P}{\pi w^2} \tag{4}$$

is the maximum beam intensity (at its center). An atom that emerges from the oven at $\vec{r} = (0, y_0, z_0)$ with speed $\vec{v} = (v_x, v_y, v_z)$ moves in relation to the laser beam, and therefore sees an intensity that is a function of time, $I(x(t), y(t))$, and consequently a saturation parameter $s_0(x, y)$ also variable in time. At the center of the beam, we have the maximum possible saturation, $s_0(L, 0) = I_c/I_{\text{sat}} = 6.10^{-3}$.

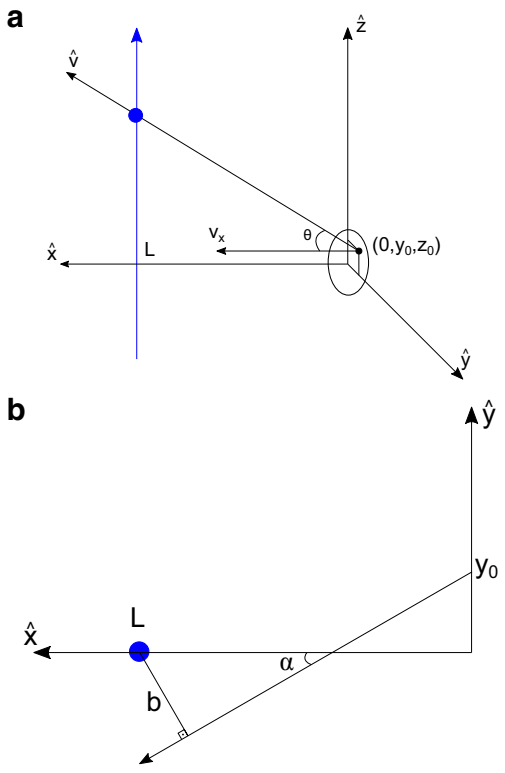

Fig. 3 **a** Experimental scheme. Atoms emerge from the oven at $\vec{r} = (0, y_0, z_0)$, with velocities distributed around the direction $\hat{x}$. A collimated laser beam, propagating in the direction $\hat{z}$ and crossing the point $(x_{\text{laser}}, 0, 0)$, makes the atoms of the atomic beam fluoresce. **b** Projection of figure (**a**) in the xy plane. The initial position of an atom projected in this plane is given by the projection of its initial position when emerging from the oven, $(0, y_0)$. The laser beam orthogonally crosses the plane at the point $(L, 0)$

We see, therefore, that the total amount of photons spread by an atom that crosses the beam depends on the trajectory of that atom. In what follows, we will assume that the variation in the speed of the atom during its trajectory, due to the absorption of photons from the laser beam, is negligible. After calculating the number of photons scattered under these conditions, we will verify this hypothesis. In addition, we neglect the effects of gravity g, since the free fall of an atom of average thermal velocity, $v_{\text{rms}} = \sqrt{k_B T/m} \simeq 280$ m/s (with k_B the Boltzmann constant and m the mass of the atom), during its movement to the laser beam, distant from $x_{\text{laser}} = 22$ cm from the oven output, is only $g/2x_{\text{laser}}^2/v_{\text{rms}}^2 = 3\,\mu$m. Thus, we assume that each atom has a constant velocity, and the projection of its trajectory on the (x, y) plane is a line, represented in Fig. 3b. We call b the distance from this line to the point $(L, 0)$, which represents the shortest distance the atom reaches from the center of the laser beam. Calling $t = 0$ the instant the atom reaches this point, the distance $s(t)$ between the atom and the center of the beam at any instant satisfies $s^2(t) = (xL)^2 + y^2 = b^2 + (v_x^2 + v_y^2)t^2$, and therefore the light intensity seen by the atom is a function of time according to:

$$s_0(t) = \frac{I(x(t), y(t))}{I_{\text{sat}}} = \frac{I_c \mathrm{e}^{-2b^2/w^2}}{I_{\text{sat}}}\, \mathrm{e}^{-2(v_x^2+v_y^2)t^2/w^2}\,. \tag{5}$$

In the atom reference frame, the laser frequency ω is different from its frequency ω_L in the laboratory frame due to the Doppler effect. They are related for non-relativistic speeds by $\omega = \omega_L(1 - v_z/c)$, so that the detuning seen by the atom is a function of v_z according to $\Delta(v_z) = \omega_L - \omega_0 - \omega_L v_z/c \simeq \Delta_0 - \omega_0 v_z/c$, with $\Delta_0 = \omega_L - \omega_0$ the detuning seen by an atom with no speed in the z direction (where we used $\omega_L \simeq \omega_0$ for detunings much smaller than the absolute frequency, $|\Delta_0| \ll \omega_L, \omega_0$: for this experiment, $|\Delta_0|/\omega_0 \lesssim 10^{-8}$). Thus, the photon scattering rate spread by the atom is a function of b, t, and $\vec{v}$, and it is written as:

$$\gamma(t, \vec{v}, b) = \frac{\Gamma}{2}\, \frac{\frac{I_c \mathrm{e}^{-2b^2/w^2}}{I_{\text{sat}}}\, \mathrm{e}^{-2(v_x^2+v_y^2)t^2/w^2}}{1 + \frac{I_c \mathrm{e}^{-2b^2/w^2}}{I_{\text{sat}}}\, \mathrm{e}^{-2(v_x^2+v_y^2)t^2/w^2} + \frac{4\Delta(v_z)^2}{\Gamma^2}}\,. \tag{6}$$

The total number of photons N_{ph} scattered by an atom when crossing the light beam is calculated from the scattering rate according to:

$$N_{\text{ph}}(\vec{v}, b) = \int_{-\infty}^{\infty} \gamma(t, \vec{v}, b)\, \mathrm{d}t \tag{7}$$

or

$$N_{\text{ph}} = \frac{\sqrt{\pi}}{2\sqrt{2}}\, \frac{w\Gamma}{\sqrt{v_x^2 + v_y^2}} \left[-\mathrm{Li}_{1/2}\left(-\frac{\frac{I_c}{I_{\text{sat}}} e^{-2b^2/w^2}}{1 + \frac{4\Delta^2(v_z)}{\Gamma^2}} \right) \right]\,, \tag{8}$$

where $\mathrm{Li}_{1/2}$ is the polylogarithmic function (also called the Joncquière function) of order $1/2$ [26]. Since the maximum

saturation parameter $I_c/I_{\text{sat}} = 6.10^{-3} \ll 1$, we can eliminate the light intensity term in the denominator of (6), and the number of atoms scattered in this low saturation limit becomes:

$$N_{\text{ph}} \approx \frac{\sqrt{\pi}}{2\sqrt{2}} \frac{w\Gamma}{\sqrt{v_x^2+v_y^2}} \frac{\frac{I_c}{I_{\text{sat}}} e^{-2b^2/w^2}}{1+\frac{4\Delta^2(v_z)}{\Gamma^2}}. \tag{9}$$

Considering the situation of maximum scattering of photons, i.e., $b = 0$ and $\Delta = 0$, an atom with thermal root mean square velocity v_{rms} scatters $N_{\text{ph,max}} = 22$ photons during its passage by the laser beam. Since the moment of one photon is h/λ_0, this corresponds to an average velocity variation of $\Delta v = N_{\text{ph,max}} h/(\lambda_0 m) = 0.21$ m/s, which is negligible with respect to the initial velocity of the atom and with respect to the typical width of the velocity class of atoms that are in resonance with the laser light, $\Delta v_D = \lambda_0\Gamma/(2\pi) = 14$ m/s. Thus, both from the point of view of the atomic resonance and trajectory, the constant velocity approximation is excellent, justifying a posteriori the calculation that allowed us to obtain (9).

Geometric considerations from Fig. 3b allow us to calculate the parameter b as a function of the parameters of the atomic motion: The initial position (y_0, z_0) in the plane $x = 0$ (representing the output of the microtubes) from which the atom leaves the oven, and its velocity $\vec{v}$. It is given by:

$$b = L\sin(\alpha) + \frac{y_0}{\cos(\alpha)} = \frac{(v_x^2+v_y^2)y_0 + v_x v_y L}{v_x\sqrt{v_x^2+v_y^2}}, \tag{10}$$

where $\alpha = \arccos(v_x/\sqrt{(v_x^2+v_y^2)})$ is the angle between the velocity of the atom in the xy plane and the x direction, shown in Fig. 3b.

3.2 Velocity Distribution of the Atomic Beam

The metallic strontium contained in our oven is kept at a high temperature to increase the saturating vapor pressure of the atomic species. At the output of the oven, we installed a system of microtubes that increase the collimation of the extracted atomic beam. If the output of the atomic oven was, instead, a simple aperture in a wall of negligible thickness, the output velocity distribution, called the effusive beam distribution $\mathcal{F}_{\text{ef}}$, would be a simple function of the velocity distribution of the thermal gas inside the oven. This velocity distribution is given by the Maxwell-Boltzmann [27] distribution, which gives the probability of finding a gas atom with velocity $v = \sqrt{v_x^2+v_y^2+v_z^2}$ of modulus between v and $v+\mathrm{d}v$ and within the infinitesimal solid angle $\mathrm{d}\Omega = \sin\theta\,\mathrm{d}\theta\,\mathrm{d}\phi$ around the direction determined by the angles $\theta = \arccos(v_x/v)$ that the velocity makes with the axis x (the axis perpendicular to the output aperture), and $\phi = \arctan(v_z/v_y)$ the angle between the projection of the speed in the yz plane and the y axis:

$$P(v,\theta,\phi)\,\mathrm{d}v\,\mathrm{d}\Omega = \frac{v^2}{(2\pi)^{3/2}\,v_{\text{rms}}^3} e^{-v^2/2v_{\text{rms}}^2}\,\mathrm{d}v\,\mathrm{d}\Omega \tag{11}$$

Looking at Fig. 4, we see that the (v,θ,ϕ) velocity atoms that are contained in a volume $\mathrm{d}V = \mathrm{d}h\,\mathrm{d}S$, with $\mathrm{d}h = \cos\theta\,\mathrm{d}l = \cos\theta\, v\,\mathrm{d}t$, they will all cross the area $\mathrm{d}S$ of the output aperture at a time $\mathrm{d}t$. Calling n the gas density, we have within the volume $\mathrm{d}V$ a total amount of atoms $n\,\mathrm{d}V$. Thus, the amount of atoms $\mathrm{d}N$ that crosses the aperture in a time $\mathrm{d}t$ and area $\mathrm{d}S$, in the differential element of velocity $\mathrm{d}v\,\mathrm{d}\Omega$ is given by:

$$\mathrm{d}N = n\,\mathrm{d}V\,P(v,\theta,\phi)\,\mathrm{d}v\,\mathrm{d}\Omega = n\,v\,\cos\theta\;\mathrm{d}t\;\mathrm{d}S\,P(v,\theta,\phi)\,\mathrm{d}v\,\mathrm{d}\Omega \tag{12}$$

The flow of atoms is defined by the number of atoms per time and area. Thus, the effusive atomic flow in the velocity differential element $\mathrm{d}v\,\mathrm{d}\Omega$ is given by:

$$\mathcal{F}_{\text{ef}}(\theta, v)\,\mathrm{d}v\,\mathrm{d}\Omega = \frac{\mathrm{d}N}{\mathrm{d}t\,\mathrm{d}S} = \frac{n}{(2\pi)^{3/2}}\frac{v^3}{v_{\text{rms}}^3} e^{-v^2/2v_{\text{rms}}^2}\cos(\theta)\,\mathrm{d}v\,\mathrm{d}\Omega = \mathcal{V}_{\text{ef}}(v)\;\mathcal{Q}_{\text{ef}}(\theta)\;\mathrm{d}v\,\mathrm{d}\Omega \tag{13}$$

The flow velocity distribution can thus be written as the product of two independent distributions in θ and v, $\mathcal{Q}_{\text{ef}}(\theta) = \cos(\theta)$ and $\mathcal{V}_{\text{ef}}(v) = \mathcal{F}_{\text{ef}}/\mathcal{Q}_{\text{ef}}$.

The presence of microtubes at the oven output causes changes in the velocity profile and in the total quantity of atoms emitted. In the general case, no analytical formula is known to describe it [23]. For a high oven pressure, it must be a function of the velocity profile of the atoms after undergoing collisions with the walls of the microtubes

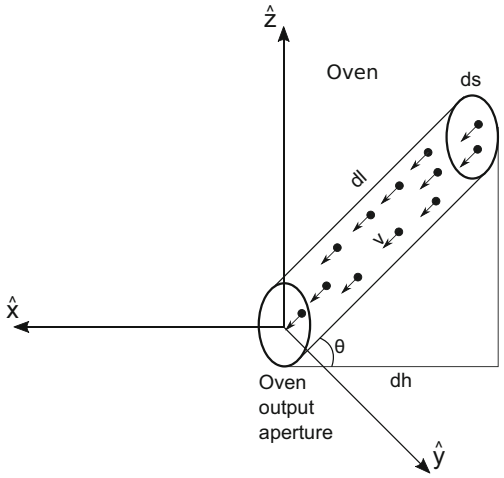

Fig. 4 Illustration of the calculation of the velocity distribution of an effusive atomic beam, for a oven with thin walls and neglecting collisions among atoms

and within themselves. In order to obtain an approximate analytical form, we will make use of some simplifying assumptions. Thus, we assume that the flow $\mathcal{F}$ exiting the microtubes at the oven output is still a product of independent distributions for θ and v, $\mathcal{F}(v,\theta) = \mathcal{V}(v)\mathcal{Q}(\theta)$, and that $\mathcal{V}$ preserves the same form as $\mathcal{V}_{\text{ef}}(v)$, apart from an overall decrease in total flow, independent of v. These hypotheses are reasonable if the walls of the microtubes are at the same temperature as the atoms in the oven, as the collisions between the gas atoms and the microscopic constituents of the walls in this case do not alter the thermal distribution of velocities of the atoms. We write, then:

$$\begin{aligned}\mathcal{F}(\theta, v)\,\mathrm{d}v\,\mathrm{d}\Omega &= \mathcal{V}(v)\,\mathcal{Q}(\theta)\;\mathrm{d}v\,\mathrm{d}\Omega \\ &= \mathcal{F}_0 \frac{v^3}{v_{\text{rms}}^3} e^{-v^2/v_{\text{rms}}^2}\mathcal{Q}(\theta)\,\mathrm{d}v\,\mathrm{d}\Omega\,, \end{aligned} \tag{14}$$

where $\mathcal{F}_0$ is now a constant which is a complicated function of the density of atoms in the furnace [23]. The behavior of $\mathcal{Q}(\theta)$ is in principle unknown. It is intuitively expected to be maximum for $\theta = 0$ and to fall to zero at $\theta = \pi/2$. The width of this curve represents the degree of collimation of the atomic beam. In order to obtain an estimate of this collimation, we used the family of functions $\mathcal{Q}_n(\theta) = \cos^n(\theta)$ to adjust our experimental data. Figure 5 shows plots of $\mathcal{Q}_n(\theta)$ for different n. For $n \to \infty$, $\mathcal{Q}_n(\theta) = \cos^n(\theta) \to \mathrm{e}^{-n\theta^2/2}$, and therefore the width at mid-height of the curve tends to $\Delta\theta = \sqrt{2\ln 2/n}$. We see, therefore, that the $\mathcal{Q}_n(\theta)$ functions allow us to describe both the effusive beam behavior, for $n = 1$, and the approximate behavior of a strongly collimated beam, for $n \gg 1$. The parameter n, from which we will deduct the angular width, will be a free parameter of the adjustment.

3.3 Effective Diameter and Position of the Oven

The hypothesis of rectilinear movement starting from the oven output implies a simple geometric relation between the velocities v_x and v_z, and the position z at which the atom crosses the laser beam: $z - z_0 = Lv_z/v_x$. In particular, this equation tells us that the only atoms that can be in resonance with the laser light when $\Delta_0 = 0$, that is, those of speed $v_z = 0$, will pass through the laser at $z = z_0$, which is the same z coordinate they had when they left the oven. As the oven has an opening of diameter 4 mm, this strongly limits the z coordinates where we can find atoms with $v_z = 0$. However, our experimental data shows that the range of positions z where this happens is actually much larger (as will be made clear in the next section). There are two hypotheses that can explain the phenomenon. The first is to consider that the atomic beam that leaves the oven has low collimation, and that in this way, many of the atoms firstly stick to the walls of the tube immediately after the microtubes, shown in Fig. 1b. These atoms would in turn be continuously re-emitted by these walls, in dynamic equilibrium, since these walls are at a temperature similar to that of the oven. The second hypothesis is to consider that the density of the atomic flux emerging from the oven is still high enough, so that the atoms continue to collide with each other during the initial propagation in the vacuum chamber, and is described in Fig. 6. These collisions would then cause a redistribution of atomic velocities after leaving the oven. In both cases, the consequence for our model is that the atoms can no longer be considered in rectilinear motion from the oven output. In order to take this into account in our model, we then assume that the parameters L, y_0, and z_0 have a different meaning than in a model without collisions. L is now no longer the distance from the laser beam to the oven output, but the distance from the laser to a plane from which the atomic motion is rectilinear. In the case of reemission of atoms from the walls of the tube external to the oven, this plane corresponds to the outer extremity of this tube; if, on the other hand, if collisions occur among atoms, this plane represents a typical x position, from which collisions become irrelevant, and propagation approximately straight. Likewise, the parameters y_0 and z_0

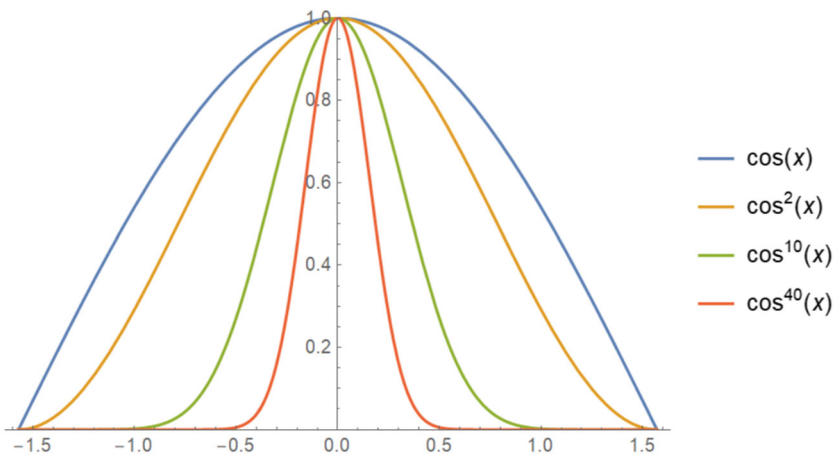

Fig. 5 Plots of $\mathcal{Q}_n(\theta) = \cos^n(\theta)$ for different n. The half-height width of these curves tends, for high n, to $\Delta\theta = \sqrt{2\ln 2/n}$

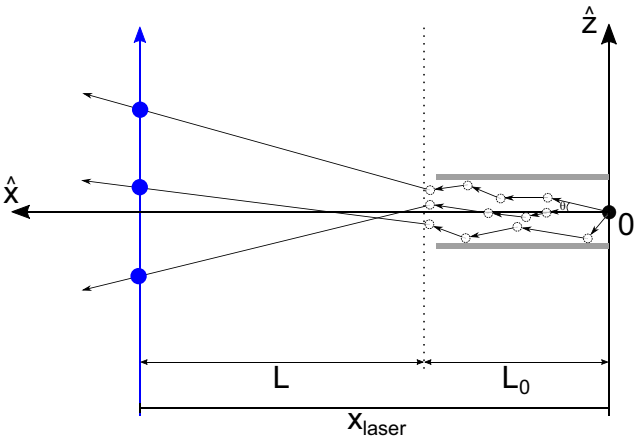

Fig. 6 Schematic representation of the atomic propagation after leaving the oven. In the occurrence of collisions between atoms during the initial propagation, or collisions between atoms and the walls of the tube (shown in gray) immediately after leaving the oven, the parameters L, y_0, and z_0 in our model represent, respectively, the distance on the x axis traveled by the atoms in a rectilinear motion, and the positions y and z where they were at the beginning of the rectilinear motion. The dashed line represents the effective beginning of the rectilinear motion of the atoms within the atomic beam. The solid blue line represents the laser beam used for measurements

do not represent the position of the atom in $x = 0$, but they are the transverse positions in the plane that determines the beginning of the linear propagation. We represent in Fig. 6 the distance L from this plane to the laser beam (where we measure the atomic fluorescence), and the distance $x_{\text{laser}} = 22$ cm between the laser beam and the oven output; thus, the plane that determines the origin of the linear propagation is at $x = x_{\text{laser}} - L$ from the oven output.

The exact form of the distribution of positions y_0 and z_0 of the atoms will depend on which one of the hypotheses above is relevant to the description of our physical system; and, moreover, it would not be easy to obtain an expression for it, since we would have to model the collisions of the atoms with each other, or the re-emission of the walls of the tube external to the oven. In order to obtain semi-quantitative information regarding the typical size of this issue, we assume for the statistical distribution function of y_0 and z_0 a Gaussian $A_\delta(y_0)$, $A_\delta(z_0)$, which has the same typical size δ in both directions due to the cylindrical symmetry of the system:

$$A_\delta(\chi) = \mathrm{e}^{-\frac{\chi^2}{\delta^2}} \tag{15}$$

4 Analysis of Experimental Data

Figure 7a shows images of the atomic fluorescence obtained from the described experimental scheme, for different detunings of the laser light. Since the signal from the

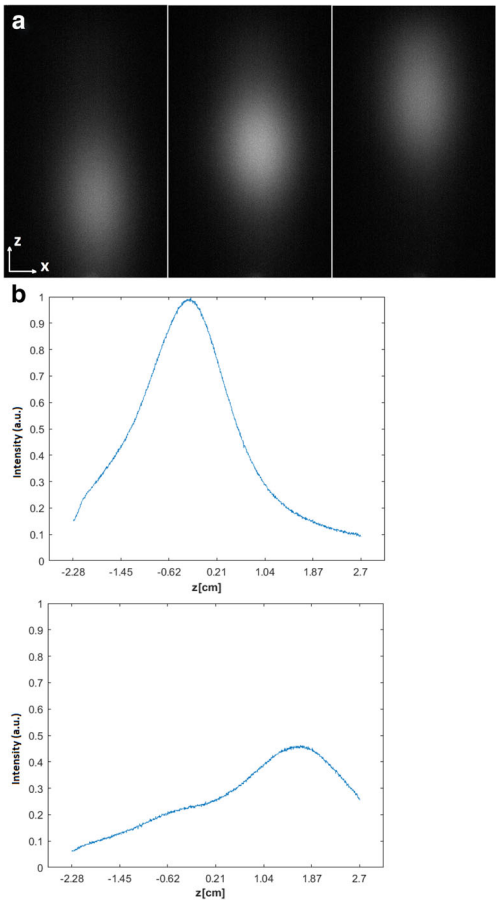

Fig. 7 **a** Example of an atomic fluorescence image captured by our CCD camera. Each image corresponds to a different detuning of the laser. **b** The integral of the image signal in the x-direction gives us fluorescence graphs as a function of the z position. The graph above is for a 4-MHz laser detuning, while the one below is for –93-MHz detuning

CCD camera is a linear function of the light intensity that impinges onto the CCD chip, and because it intercepts practically the same solid angle of the light emitted by atoms in any position of the beam, the signal in each pixel is directly proportional to the amount of light emitted by all the atoms that passed in all the spatial points imaged in that pixel, integrated during the camera's exposure time and in the direction $\hat{y}$, normal to the image plane. As the size w of the beam is much smaller than the distance L of the beam at the exit of the oven (see Fig. 6), the variation of the z coordinate of the atoms during their passage through the light is small, and we neglect it in order to simplify data analysis. Thus, we make the integral of the images in the x direction, obtaining an atomic fluorescence curve as a function of the camera's z coordinate, shown in Fig. 7b, so that, at the end, our data set to be analyzed is a two-dimensional $M(z, \Delta_0)$, atomic fluorescence matrix as a function of Δ_0 and z. The procedure of capturing images for

different detunings is essential to be able to observe all the velocity classes present in the atomic beam.

In order to obtain the beam divergence, as well as the geometric parameters L and δ of the atomic trajectories, we fitted the experimental data to the expected theoretical fluorescence profile as a function of z and Δ_0. We obtain this profile by calculating the total number of photons emitted by an atom in the low saturation approach, (9), and the distribution of atomic velocities, (14). In the steady state, the flow is constant throughout the space, and we can calculate the fluorescence rate of the atoms whose speed is contained in the differential element $v^2\,\mathrm{d}v\,\mathrm{d}\Omega = \mathrm{d}v_x\,\mathrm{d}v_y\,\mathrm{d}v_z$ as simply the total number of photons emitted by an atom times the emission rate of atoms in this differential volume:

$$\gamma(\Delta_0, n, L, y_0, \vec{v})\,\mathrm{d}v\,\mathrm{d}\Omega = \mathcal{K}_0 \frac{I_c}{I_{\mathrm{sat}}} \frac{w\Gamma}{\sqrt{v_x^2+v_y^2}} \frac{e^{-\frac{2\left[(v_x^2+v_y^2)y_0+v_x v_y L\right]^2}{w^2 v_x^2(v_x^2+v_y^2)}}}{1+\frac{4\Delta^2(v_z)}{\Gamma^2}} \frac{v}{v_{\mathrm{rms}}^3} e^{-\frac{v^2}{2v_{\mathrm{rms}}^2}} \mathcal{Q}_n(\arccos(\tfrac{v_x}{v}))\,\mathrm{d}v_x\,\mathrm{d}v_y\,\mathrm{d}v_z \tag{16}$$

In the equation above, we use the expression of b given by the (10), and also the definition of θ, $\theta = \arccos(v_x/v)$. The $\mathcal{K}_0$ constant includes the $\mathcal{F}_0$ constant, numerical factors, camera detection efficiency, solid detection angle, and global normalization of the curves. The collimation of the atomic beam is a function of the parameter n; of the temperature T through v_{rms} dependency on T; and of the laser detuning Δ_0 contained in the expression for $\Delta(v_z)$. For an integration time Δt, the total amount of photons emitted by the atoms with velocity contained in $\mathrm{d}v\,\mathrm{d}\Omega$ will simply be the amount above multiplied by Δt.

The rectilinear movement of the atoms allows us to deduce a geometric relationship between their velocities and the displacements, $z - z_0$ and L, respectively in z and x:

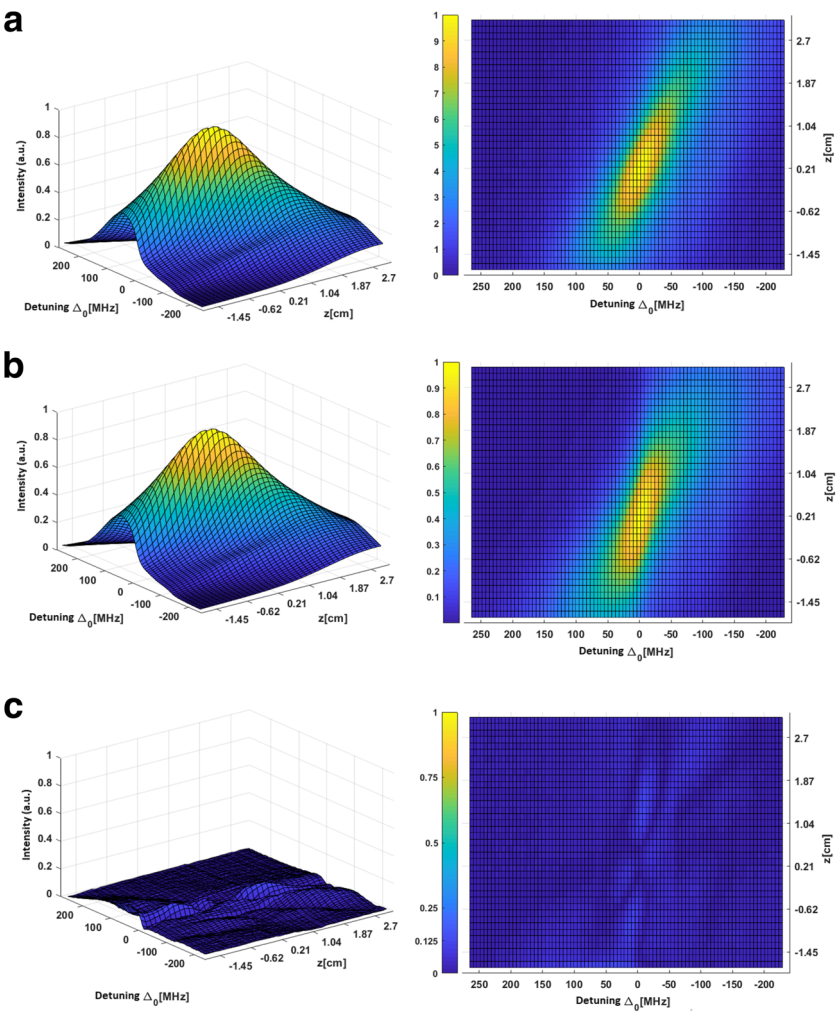

Fig. 8 **a** Matrix $M(z, \Delta_0)$ of experimental atomic fluorescence, normalized to its largest value. **b** Theoretical curve, $N(z, \Delta_0, n, L, \delta)$, given by (17), adjusted to the experimental data. **c** Absolute value of the difference between both, $|M(z, \Delta_0) - N(z, \Delta_0, n, L, \delta)|$, after fitting of experimental data to the theoretical curve. To the right of each graph, we see its projection on the z, Δ_0 plane

$z = z_0 + L\frac{v_z}{v_x}$. We use this relationship to replace v_z in (16). In order to obtain the total fluorescence as a function of z, Δ_0 and the free adjustment parameters, n, L, and δ, we have integrated the eq emission rate. Equation (16) in v_x, v_y, y_0, and z_0, according to the distribution of starting positions given by (15), and if we multiply by the time Δt of camera integration, we finally obtain an expression for the detected total fluorescence, to be used in the numerical adjustment:

$$N(z,\Delta_0,n,L,\delta)\,\mathrm{d}z = K_0\Delta t\left(\frac{m}{k_BT}\right)^{\frac{3}{2}}\frac{I_c}{I_{\mathrm{sat}}}\int_{-\infty}^{\infty}\mathrm{d}y_0\,A_\delta(y_0)\int_{-\infty}^{\infty}\mathrm{d}z_0\,A_\delta(z_0)\int_{-\infty}^{\infty}\mathrm{d}v_x\int_{-\infty}^{\infty}\mathrm{d}v_y \frac{w\Gamma}{\sqrt{v_x^2+v_y^2}}\frac{e^{-\frac{2\left[(v_x^2+v_y^2)y_0+v_xv_yL\right]^2}{w^2v_x^2(v_x^2+v_y^2)}}}{1+4\left(\frac{\Delta_0-\frac{\omega_0v_x(z-z_0)}{cL}}{\Gamma}\right)^2}\frac{v_x^n e^{-\frac{m\left[v_x^2\left(1+\left(\frac{z-z_0}{L}\right)^2\right)+v_y^2\right]}{2k_BT}}}{\left[v_x^2\left(1+\left(\frac{z-z_0}{L}\right)^2\right)+v_y^2\right]^{\frac{n-1}{2}}}\mathrm{d}z \tag{17}$$

We did a numerical fitting of the function $N(z, \Delta_0, n, L, \delta)$ to our two-dimensional array of experimental data $M(z, \Delta_0)$ with a MATLAB routine that minimizes the quadratic distance between both as a function of n, L, and δ. Figure 8a shows the matrix M, and in (b), we have the function N calculated for the parameters n, L, and δ found for the fitting. The difference between them in absolute value is shown in Fig. 8c, which shows that the adjustment error does not exceed 15% of the maximum fluorescence value. The simplifications used in obtaining the (17) justifies the lack of better agreement between both. The value of the parameters found with this adjustment is $n = 37$, $L = 14.7$ cm, and $\delta = 9.3$ mm.

The value of the parameter n allows us to estimate the typical width of the divergence, since the half width at $1/e$ of the curves $Q_n(\cos\theta)$ is $\Delta\theta = \sqrt{2/n} = 0.23$ rad $= 13°$. At the low-pressure limit, the divergence of the atomic beam from the microtubes should be in the order of $d/l \sim 0.016$ rad $= 0.9°$; we see, therefore, that we are in the regime in which collisions during the propagation through the microtubes cannot be neglected. The parameters L and δ, on the other hand, give us information about what happens to the atoms right after they emerge from the oven. We see that δ has a value reasonably greater than 2 mm, which is the radius of the oven output aperture, shown in Fig. 2, where the microtubes are installed; likewise, $L < 22$ cm, which is the distance between the oven output plane and the center of the laser beam. This shows that the atomic velocities are likely to be redistributed during the atomic trajectory after the oven output. It is interesting to note that the adjustment of our data tells us that the distance from the oven output to the beginning of the atomic rectilinear movement is equal to $x_{\mathrm{laser}} - L = 7.3$ cm, which corresponds almost exactly to the length of the tube located in front of the oven, which is 6.9 cm. Likewise, the radius of this tube is 6.5 mm, close to $\delta = 9.3$ mm. This indicates that this tube probably has an influence on this speed redistribution. It is likely that the beam divergence would be even greater, were it not for the presence of this tube, with part of the atoms initially colliding with its walls, being trapped there and reemitted later in a random direction; which does not eliminate possible effects of collisions among atoms, that can also take place during their propagation.

5 Conclusion

In this article, we describe a characterization of the distribution of directions of the velocity of atoms leaving an atomic oven. This measurement was performed through the detection of atomic fluorescence, produced by the excitation of the atoms with a narrowband, quasi-resonant laser beam, which crosses the atomic beam perpendicularly. An important feature for the interpretation of the experiment data is that the width of the dipolar atomic transition used, Γ, is much smaller than the typical Doppler dispersion of the resonant frequencies $\Delta_D = \omega_0 v_{\mathrm{rms}}/c = \omega_0/c\sqrt{k_BT/m}$; in our case, $\Gamma = 2\pi \times 30.5$ MHz and $\Delta_D \simeq 2\pi \times 610$ MHz. This means that this characterization can only be done though a scan of the laser detuning, in order to observe all the different atomic velocity classes present in the atomic beam. The experimental data thus obtained correspond to a two-dimensional matrix, function of the position z in which the atoms pass through the laser beam and the light detuning Δ_0. In order to deduce the relevant geometric quantities of our atomic beam, a theoretical model was developed from elementary considerations about the scattering of light by a diluted atom gas and the velocity distribution profile of the atoms that emerge from the oven. We have assumed ad hoc functions to approximately describe the distributions of initial transversal position and velocity direction of the atoms; these functions depend on parameters that were deduced from the fitting of the theoretical model to the experimental data. This procedure allowed us to obtain a value for the average beam divergence and also to identify the presence of velocity redistribution processes during the atomic propagation after the oven output aperture, such as collisions with the container walls and with other atoms from the atomic beam. This fact prevented us from linking the atomic divergence obtained to the microtube behavior only.

Acknowledgments The authors would like to thank Cleber Renato Mendonça and Jonathas de Paula Siqueira, from the Photonics group at IFSC-USP, for cutting the microtubes.

Funding The authors acknowledge the funding through FAPESP projects 2013/04162-5, FAPESP 2018/00221-0, and FAPESP 2015/25146-3.

References

1. T.W. Hänsch, A.L. Schawlow, Cooling of gases by laser radiation. Opt. Commun. **13**, 68 (1975)
2. P.D. Lett, W.D. Phillips, S.L. Rolston, C.E. Tanner, R.N. Watts, C.I. Westbrook, Optical molasses. JOSA B **6**, 2084 (1989)
3. W.D. Phillips, H. Metcalf, Laser deceleration of an atomic beam. Phys. Rev. Lett. **48**, 596 (1982)
4. E.L. Raab, M. Prentiss, A. Cable, S. Chu, D.E. Pritchard, Trapping of neutral sodium atoms with radiation pressure. Phys. Rev. Lett. **59**, 2631 (1987)
5. J. Dalibard, C. Cohen-Tannoudji, Laser cooling below the Doppler limit by polarization gradients: simple theoretical models. JOSA B **11**, 2023 (1989)
6. A.M. Steane, C.J. Foot, Laser cooling below the Doppler limit in a magneto-optical trap. EPL **14**, 231 (1991)
7. C.h. Monroe, D.M. Meekhof, B.E. King, S.R. Jefferts, W.M. Itano, D.J. Wineland, P. Gould, Resolved-sideband Raman cooling of a bound atom to the 3D zero-point energy. Phys. Rev. Lett. **75**, 4011 (1995)
8. M.H. Anderson, J.R. Ensher, M.R. Matthews, C.E. Wieman, E.A. Cornell, Observation of Bose-Einstein condensation in a dilute atomic vapor. Science **269**, 198 (1995)
9. K.B. Davis, M.-O. Mewes, M.R. Andrews, N.J. Van Druten, D.S. Durfee, D.M. Kurn, W. Ketterle, Bose-Einstein condensation in a gas of sodium atoms. Phys. Rev. Lett. **75**, 3969 (1995)
10. A.G. Truscott, K.E. Strecker, W.I. McAlexander, G.B. Partridge, R.G. Hulet, Observation of Fermi pressure in a gas of trapped atoms. Science **291**, 2570 (2001)
11. I.B. Spielman, W.D. Phillips, J.V. Porto, Mott-insulator transition in a two-dimensional atomic Bose gas. Phys. Rev. Lett. **98**, 080404 (2007)
12. I. Ferrier-Barbut, H. Kadau, M. Schmitt, M. Wenzel, T. Pfau, Observation of quantum droplets in a strongly dipolar Bose gas. Phys. Rev. Lett. **116**, 215301 (2016)
13. J. Billy, V. Josse, Z. Zuo, A. Bernard, B. Hambrecht, P. Lugan, D. Clément, L. Sanchez-Palencia, P. Bouyer, A. Aspect, Direct observation of Anderson localization of matter waves in a controlled disorder. Nature **453**, 891 (2008)
14. W. Guerin, M.O. Araújo, R. Kaiser, Subradiance in a large cloud of cold atoms. Phys. Rev. Lett. **116**, 083601 (2016)
15. K.L. Moore, T.P. Purdy, K.W. Murch, S. Leslie, S. Gupta, D.M. Stamper-Kurn, Collimated, single-pass atom source from a pulsed alkali metal dispenser for laser-cooling experiments. Rev. Sci. Instrum. **76**, 023106 (2005)
16. H. Brand, B. Nottbeck, H.H. Schulz, A. Steudel, Laser-atomic-beam spectroscopy in the samarium I spectrum. J. Phys. B: Atom. Molecul. Phys. **11**(4), L99 (1978)
17. J.E. Thomas, P.R. Hemmer, S.h. Ezekiel, JrC.C. Leiby, R.H. Picard, C.R. Willis, Observation of Ramsey fringes using a stimulated, resonance Raman transition in a sodium atomic beam. Phys. Rev. Lett. **48**, 867 (1982)
18. D.J. Glaze, H. Hellwig, D.W. Allan, S. Jarvis, NBS-4 and NBS-6: The NBS primary frequency standards. Metrologia **13**(1), 17 (1977)
19. J.P. Gordon, H.J. Zeiger, C.h.H. Townes, The maser—new type of microwave amplifier, frequency standard, and spectrometer. Phys. Rev. **99**, 1264 (1955)
20. H.M. Goldenberg, D. Kleppner, N.F. Ramsey, Atomic hydrogen maser. Phys. Rev. Lett. **5**, 361 (1960)
21. W. Happer, Optical pumping. Rev. Mod. Phys. **44**, 169 (1972)
22. R.E. Grove, F.Y. Wu, S. Ezekiel, Measurement of the spectrum of resonance fluorescence from a two-level atom in an intense monochromatic field. Phys. Rev. A **15**, 227 (1977)
23. C.B. Lucas, The production of intense atomic beams. Vacuum **23**, 395 (1973)
24. P.H. Moriya, M.O. Araújo, F. Todão, M. Hemmerling, H. Keßler, R.F. Shiozaki, R. Celistrino Teixeira, Ph.W. Courteille, Comparison between 403 nm and 497 nm repumping schemes for strontium magneto-optical traps. J. Phys. Commun. **2**, 125008 (2018)
25. F.ritz. Riehle, Frequency Standards: Basics and Applications. Wiley (2006)
26. A. Erdélyi, W. Magnus, F. Oberhettinger, F.G. Tricomi, Vol. 1, *Higher Transcendental Functions* (Krieger, New York, 1981), pp. 30–31
27. R.A. Salinas Sílvio, Introdução à física estatística. Edusp (1997)